

Cite this article as: Jiang Lianyun, Huang Jinbo, Zhen Tao, et al. Analytical Modeling of Plate Curvature in Snake Rolling of Heavy Aluminum Alloy with Different Deformation Zones[J]. Rare Metal Materials and Engineering, 2021, 50(05): 1626-1634.

ARTICLE

Analytical Modeling of Plate Curvature in Snake Rolling of Heavy Aluminum Alloy with Different Deformation Zones

Jiang Lianyun¹, Huang Jinbo¹, Zhen Tao¹, Le Qichi², Ma Lifeng¹

¹ School of Mechanical Engineering, Taiyuan University of Science and Technology, Taiyuan 030024, China; ² Key Laboratory of Electromagnetic Processing of Materials, Ministry of Education, Northeastern University, Shenyang 110819, China

Abstract: The snake rolling manufacture technique provides a new method for producing high-performance heavy aluminum plates. The traditional curvature model of the asymmetrical rolling cannot be simply applied to calculate the curvature of the snake rolling. The plate curvature model of the snake rolling was set up in this research according to the roll offset and different roll radii. The deformation region consists of four different zones at most which depends on the positions of the two neutral points, and this number may drop to three or two under other conditions. The deformation zone with different composition cases was analyzed, and the models of the specific pressure and the accumulated shear strain deviation between the upper and lower parts of the plate were established. The plate curvature caused by shear strain and axial strain was calculated separately. The homogeneity coefficient E was introduced during the plate curvature modeling process to ensure the model accuracy. Then the total plate curvature model was established. Ansys software simulation can well restore the snake rolling process, and the indirect experiments were also conducted to verify the precision of plate curvature theoretical model. The results show that the maximum and minimum relative error is 10.71% and 0.34%, respectively, compared to results of simulation method and the indirect experiments, indicating that the model can be applied for the online plate curvature control application with the effect of some self-learning methods. The plate curvature affecting law with different process parameters (roll offset, roll radius ratio, rolling reduction, and initial work piece thickness) was obtained. This research about the plate curvature modeling provides important references for the production of heavy aluminum plate snake rolling.

Key words: snake rolling; curvature; neutral point; shear strain; axial strain

Aluminum alloy plate has been widely used in many aspects, especially in aerospace and modern transportation techniques due to its advantages of low density and high strength. In recent years, high-strength aluminum alloy plate has been widely used as the main structural materials in the fields of aircraft, rockets, spacecraft, and space stations^[1-3]. It has become the most promising green material. Therefore, higher requirements are put forward for the specifications of heavy plates used for high-strength and high-toughness aluminum alloy structural parts. However, the mechanical property is not very well because of the little deformation in the inner region. Because of the work roll threading ability and the total thickness of the casting slab, it is difficult to satisfy the total rolling reduction requirement. Therefore, the problem of insufficient in-

ner deformation has become the key technical obstruction to ameliorate the quality of aluminum alloy plate.

The asymmetrical rolling is a rolling process to ameliorate the plate mechanical properties. The cross shear zone forms in the roll gap during the asymmetrical rolling, which is beneficial to the deep deformation into the inner portion^[4-7]. Cui et al^[8] obtained the equiaxed fine-grained pure aluminum with a grain size of 2 μm through asymmetrical rolling, and the microstructure is continuous in specimen, and the additional shear deformation introduced by asymmetrical rolling is the main reason for the grain refinement. Wronski et al^[9] examined the crystal structure and mechanical properties of the aluminum alloy by the asymmetrical rolling. Compared with the symmetric rolling, the asymmetric rolling improves the micro-

Received date: January 07, 2021

Foundation item: National Natural Science Foundation of China (51804206); Open Research Fund from the State Key Laboratory of Rolling and Automation, Northeastern University (2020RALKFKT010)

Corresponding author: Ma Lifeng, Ph. D., Professor, School of Mechanical Engineering, Taiyuan University of Science and Technology, Taiyuan 030024, P. R. China, E-mail: mlf_zgtyust@163.com

Copyright © 2021, Northwest Institute for Nonferrous Metal Research. Published by Science Press. All rights reserved.

structure and produces uniform grain structure. Jin et al^[10] used asymmetrical rolling and annealing process to prepare 5754 aluminum alloy with a grain size of 1 μm . The grain size effect of the alloy obviously strengthens. Angella et al^[11] evaluated the possibility of commercial Al-Mg-Si alloy treated through the asymmetric rolling and accumulative rolling bonding (ARB). The experimental characterization shows that the asymmetrical rolling promotes the formation of ultrafine grain structure in the aluminum alloy.

The asymmetrical rolling has the advantage of ameliorating the central deformation, but the work piece is bent after rolling^[12]. Many scholars conducted researches on the plate curvature after asymmetrical rolling from the perspectives of the finite element method (FEM) and the experiment, and they tried to establish the law and the relationship between the plate curvature and rolling parameters in order to eliminate or reduce the plate curvature through the process optimization. Gong et al^[13] simulated the asymmetrical rolling process, and the simulated characterization demonstrates that the curvature radius reduces as the friction coefficient, friction coefficient ratio, rolling reduction or the work roll diameter increases. And the curvature radius increases with the increase of plate thickness. In addition, the plate thickness has more effects on the front curvature compared to the influence of rolling reduction. Hao et al^[14] studied the plate curvature after asymmetrical rolling caused by different roll diameters via two-dimensional finite element method, and the effect of work roll diameter mismatch was investigated as an approach to control the plate curvature. Farhatnia et al^[15] predicted the plate curvature of the asymmetrical rolling due to the inequality in work roll/plate surface finish (interface friction) and the speed mismatch by the finite element method.

Many scholars used the slab method to study the curvature after asymmetric rolling. Kadkhodaei et al^[16] conducted a slab method for the asymmetric sheet rolling. The rolling force and pressure distribution predicted by this model are in good agreement with the experimental and theoretical results. Qwamizadeh et al^[17,18] studied the plate curvature after the asymmetrical rolling by the slab method and the plate curvature of the bonded two-layer plates under different conditions was obtained. Salimi et al^[19,20] established the plate curvature model of thin strip asymmetrical rolling with different work roll diameters by the slab method. Afrouz et al^[21] used the slab method to model and study the mechanical parameters and the plate curvature for the asymmetrical rolling when the shear stress of the cold rolled strip was non-uniform. The bending of the work piece affects the flatness of the product and has a great impact on the stable operation of rolling mill.

The snake rolling is a special asymmetrical rolling process which ameliorates the central deformation and reduces the bending of the work piece. Many scholars started to investigate about the snake rolling. Ling^[22] and Zhang^[23] et al found that the snake rolling increases the magnitude and the through-thickness homogeneity of the accumulated equivalent strains compared to the effect of conventional rolling. Jiang^[24] and Yang^[25] et al investigated the bending behavior during the

snake rolling. The plate curvature of the rolled plate after the snake rolling effectively reduces by adjusting the parameters. Jiang et al^[26] established the theoretical model of mechanical parameters of the snake/gradient temperature rolling by the slab method. It is essential to study the curvature of the snake rolling.

At present, the plate curvature of the asymmetrical rolling was studied by FEM and experimental method separately, and the theoretical model of the plate curvature was established by slab method. There is a great difference between the snake rolling and the asymmetrical rolling because of different characteristics in the deformation region. The traditional theoretical model of the asymmetrical rolling cannot be simply applied to calculate the curvature of the snake rolling. The deformation region may be divided into three different situations with different neutral point positions. Therefore, it is necessary to conduct intensive study to comprehensively evaluate the snake rolling and accurately predict the plate curvature. The analysis of the plate curvature modeling provides an essential theoretical basis for the production with good shape during the snake rolling.

1 Mathematical Model

Fig. 1 shows the geometric diagram of the snake rolling with different work roll radii. The origin center of the two work rolls is not on a vertical line, and there is a roll offset d between the two work rolls. The rolled piece threads synchronously. The x axis is defined as the opposite direction of the plate moving direction, and the y axis points to the center of the top work roll. “O” point in Fig.1 is the center of the coordinate axis. Δh_1 and Δh_2 are the reductions of the upper and lower parts, respectively, which are not the same due to the roll offset. n_1 and n_2 are the angular velocity of the upper and lower work rolls, respectively, with $n_1=n_2$; R_1 and R_2 are the radii of the upper and lower work rolls, respectively, with $R_2>R_1$.

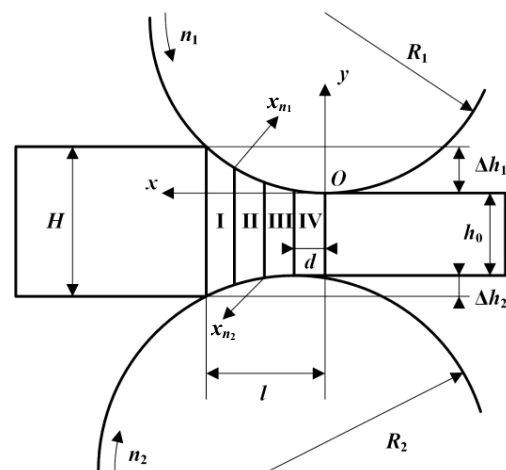


Fig.1 Geometric diagram of the snake rolling with different work roll radii

l is the deformation region length. x_{n_1} and x_{n_2} are the neutral points; H is the initial thickness; h_0 is the thickness of specimen after rolling.

Although the angular velocities $n_1=n_2$, the linear velocities of the two work rolls are not the same due to their different radii, resulting in the appearance of two neutral points at different horizontal positions: x_{n_1} and x_{n_2} . The deformation region consists of four zones at most, i.e., back slip zone I, cross shear zone II, front slip zone III and reverse deflection zone IV, as shown in Fig.2.

There are three cases when the two neutral points locate at different positions: (1) the deformation region consists of zone I, II, III and IV when x_{n_1} locates at the right side of the inlet point and x_{n_2} locates at left side of the bottom outlet point; (2) the deformation region consists of zone I, II and IV when x_{n_1} locates at right side of the inlet point and x_{n_2} locates at or beyond the bottom outlet point; (3) the deformation region consists of zone II and IV when x_{n_1} locates at or beyond the inlet point and x_{n_2} locates at or beyond the bottom outlet point.

1.1 Neutral points position

The deformation region is divided into four different zones at most depending on the position of the two neutral points, and this number drops to three or two under other conditions. The boundary conditions are $x=0$ and $q=0$ at the "O" point when all the four zones exist (x is the horizontal distance from the throw point. q is the horizontal normal stress in the deformation region). Therefore the specific pressure in zone IV is $p_{IV} = \sigma_s(\sqrt{1 - m^2 c_1^2} + \sqrt{1 - m^2 c_2^2})/\sqrt{3}$, with $c_1=c_2=0.5$. σ_s is the flow stress; m is the friction coefficient; c_1 and c_2 are the related coefficients at the top and bottom portions^[20], respectively. The integral constant C_{IV} can be confirmed by Eq.(1) as follows:

$$p_{IV} = M \ln(x^2 + 2R_1 h_0) + \frac{2Ax}{R_1} + \frac{\sqrt{2} A(R_1 - 2h_0)}{\sqrt{R_1 h_0}} \arctan \frac{x}{\sqrt{2R_1 h_0}} + C_{IV} \tag{1}$$

with dimensionless coefficients

$$M = \frac{\sigma_s}{\sqrt{3}} (\sqrt{1 - m^2 c_1^2} + \sqrt{1 - m^2 c_2^2})$$

$$A = \tau_1 = \tau_2 = m\sigma_s/\sqrt{3}$$

The boundary conditions are $x=l$, $q=0$ at the inlet point. Therefore the specific pressure in zone I is $p_1 = \sigma_s(\sqrt{1 - m^2 c_1^2} + \sqrt{1 - m^2 c_2^2})/\sqrt{3}$, with $c_1=c_2=0.5$. C_1 can be confirmed by Eq.(2) as follows:

$$p_1 = M \ln(ix^2 - 2dx + d^2 + x^2 + 2R_1 h_0 i) + 2AB \arctan \frac{x - d + ix}{\sqrt{id^2 + 2R_1 h_0 i + 2R_1 h_0 i^2}} - \frac{2Ax(i^2 + 1)}{R_1 i(i + 1)} - 2Ad(i - 1) \frac{\ln|(AB - C + D)(AB + C - D)|}{R_1(i + 1)^2} + C_1 \tag{2}$$

with $i = R_2/R_1$

$$B = (-2R_1^2 i^3 - 4R_1^2 i^2 - 2R_1^2 i + 2h_0 R_1 i^3 + 2h_0 R_1 i^2 + 2h_0 R_1 i + i^2 d^2 - 2id^2 + d^2)/((i + 1)^2 R_1 \sqrt{id^2 + 2h_0 R_1 i + 2h_0 R_1 i^2})$$

$$C = \frac{2A(-2R_1^2 i^2 - 2R_1^2 i + 2h_0 R_1 i^2 + 2h_0 R_1 + id^2 - d^2)}{R_1(i + 1)}$$

$$D = \frac{4Ad^2(i - 1)}{R_1(i + 1)^2}$$

where i is the roll radius ratio; τ_1 and τ_2 are the plate surface shear stresses at the top and bottom deformation region, respectively.

At the position of $x=x_{n_1}$, $p_I=p_{II}$, and then C_{II} can be confirmed. At the position of $x=x_{n_2}$, $p_{II}=p_{III}$, and then C_{III} can be confirmed. $c_1=c_2=1$ in zone II and $c_1=c_2=0.5$ in zone III. The specific pressures in zone II and III are described by Eq.(3) as follows:

$$\left\{ \begin{aligned} P_{II} &= [M + \frac{2Ad}{(i + 1)R_1}] \ln(ix^2 - 2dx + d^2 + x^2 + 2R_1 h_0 i) \\ &+ \frac{2Ax(i - 1)}{iR_1} - \frac{2(i - 1)AE \arctan(\frac{x - d + ix}{\sqrt{i}})E}{(i + 1)R_1 \sqrt{i}} + C_{II} \\ P_{III} &= M \ln(ix^2 - 2dx + d^2 + x^2 + 2R_1 h_0 i) \\ &- 2AB \arctan \frac{x - d + ix}{\sqrt{id^2 + 2R_1 h_0 i + 2R_1 h_0 i^2}} + \frac{2Ax(i^2 + 1)}{R_1 i(i + 1)} \\ &+ 2Ad(i - 1) \frac{\ln|(AB - C + D)(AB + C - D)|}{R_1(i + 1)^2} + C_{III} \end{aligned} \right. \tag{3}$$

with $E = \sqrt{d^2 + 2R_1 h_0 + 2R_1 h_0 i}$

The specific pressure is continuous at the neutral point, so Eq.(4) can be obtained as follows:

$$C_{II}(x = x_{n_1}) = C_{II}(x = x_{n_2}) \tag{4}$$

Eq.(5) can be obtained according to the constant volume as follows:

$$v_1 \sqrt{1 - \frac{x_{n_1}^2}{R_1^2}} [h_0 + \frac{ix_{n_1}^2 + (x_{n_1} - d)^2}{2iR_1}] = v_2 \sqrt{1 - \frac{(x_{n_2} - d)^2}{i^2 R_1^2}} [h_0 + \frac{ix_{n_2}^2 + (x_{n_2} - d)^2}{2iR_1}] \tag{5}$$

where v_1 and v_2 are the linear velocity of top and bottom work rolls, respectively. Therefore x_{n_1} and x_{n_2} can be calculated by combining the Eq.(4) and Eq.(5).

The deformation zones change from four to three (zone I, II and IV). The boundary conditions are $x=l$, $q=0$ at the inlet point. Therefore the specific pressure in zone I is $p(x = l) = \sigma_s(\sqrt{1 - m^2 c_1^2} + \sqrt{1 - m^2 c_2^2})/\sqrt{3}$. Then C_1 can be obtained by Eq.(2).

At the position of $x=d$, $p_{II}=p_{IV}$, and then C_{II} can be confirmed. At the position of $x=x_{n_1}$, $p_I=p_{II}$, and then x_{n_1} can be confirmed.

1.2 Plate curvature caused by shear strain

The shear strain causes the plate deflect during the plastic deformation. Shear strain differential of the upper and lower

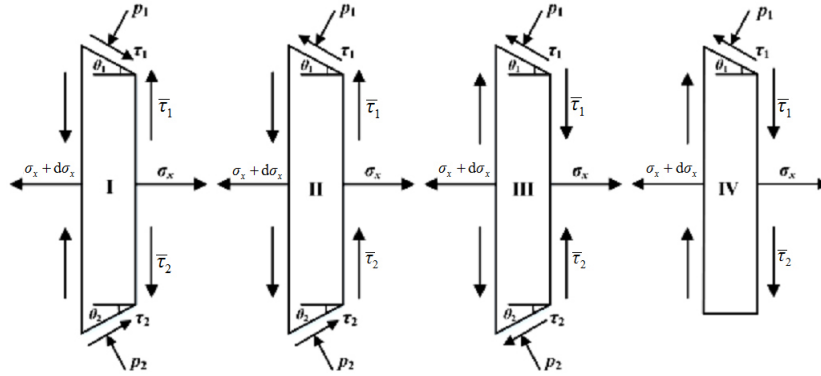


Fig.2 Stress status at different positions in plastic deformation zone

parts of the work piece can be expressed as Eq. (6) according to the flow criterion as follows:

$$\begin{cases} d\lambda_{xy1} = \tau_{xy1} d\varepsilon_{y1} / \sigma'_{y1} \\ d\lambda_{xy2} = \tau_{xy2} d\varepsilon_{y2} / \sigma'_{y2} \end{cases} \quad (6)$$

where λ_{xy1} and λ_{xy2} are the average shear strain at the top and bottom portion of the plate, respectively; τ_{xy1} and τ_{xy2} are the shear yield strength of rolled piece at the top and bottom portion, respectively; ε_{y1} and ε_{y2} are the strain of the top and bottom of rolled piece along y direction, respectively; σ'_{y1} and σ'_{y2} are the stress bias of the top and bottom parts of rolled piece along y direction, respectively.

The strain differential along y direction of the upper and lower parts of the work piece in the deformation region can be described as follows:

$$\begin{cases} d\varepsilon_{y1} = \frac{dh_1}{h_1} = \frac{2x}{R_1 h_0 + x^2} dx \\ d\varepsilon_{y2} = \frac{dh_2}{h_2} = \frac{2(x-d)}{iR_1 h_0 + (x-d)^2} dx \end{cases} \quad (7)$$

Because $\sigma_z = (\sigma_x + \sigma_y) / 2$, the hydrostatic pressure in the deformation region is $\sigma_m = (\sigma_x + \sigma_y) / 2$. The stress bias along x and y directions is expressed as follows:

$$\begin{cases} \sigma'_x = \sigma_x - \sigma_m = (\sigma_x - \sigma_y) / 2 \\ \sigma'_y = \sigma_y - \sigma_m = (\sigma_y - \sigma_x) / 2 \end{cases} \quad (8)$$

where σ'_x and σ'_y are the stress bias along x and y direction, respectively; σ_x , σ_y and σ_z are the normal stress along x , y and z axis, respectively.

Considering the average normal stresses of the upper and lower parts of the work piece, Eq. (9) can be obtained as follows:

$$\begin{cases} d\lambda_{xy1} = n_1 d\varepsilon_{y1} \\ d\lambda_{xy2} = n_2 d\varepsilon_{y2} \end{cases} \quad (9)$$

with $n_1 = c_1 m / \sqrt{1 - c_1^2 m^2}$, $n_2 = c_2 m / \sqrt{1 - c_2^2 m^2}$

The deformation region length l can be expressed as follows:

$$l = \sqrt{R_1^2 - (R_1 - \Delta h_1)^2} = \sqrt{2R_1 \Delta h_1 - \Delta h_1^2} \quad (10)$$

with $\Delta h_1 = x^2 / 2R_1$

Three cases are summarized separately. (1) Case 1 ($d < x_{n_1} < l$, $d < x_{n_2} < x_{n_1}$). The shear strains of the upper and lower parts are in opposite direction in zone I, and the shear strain of the ele-

ment can be expressed as $d\lambda_i = (d\lambda_{xy2} - d\lambda_{xy1}) / 2$. The shear strains of the element in zone II, III and IV are $d\lambda_{II} = (d\lambda_{xy2} + d\lambda_{xy1}) / 2$, $d\lambda_{III} = (d\lambda_{xy1} - d\lambda_{xy2}) / 2$ and $d\lambda_{IV} = d\lambda_{xy1} / 2$, respectively. Therefore, the accumulated shear strain deviation of the work piece in zone I, II, III and IV can be calculated by Eq. (11) as follows:

$$\begin{cases} \alpha_I = \int_{x_{n_1}}^l d\lambda_I = \frac{1}{2} \left[n_2 \ln \frac{(l-d)^2 + iR_1 h_0}{(x_{n_1}-d)^2 + iR_1 h_0} - n_1 \ln \frac{l^2 + R_1 h_0}{x_{n_1}^2 + R_1 h_0} \right] \\ \alpha_{II} = \int_{x_{n_2}}^{x_{n_1}} d\lambda_{II} = \frac{1}{2} \left[n_2 \ln \frac{(x_{n_1}-d)^2 + iR_1 h_0}{(x_{n_2}-d)^2 + iR_1 h_0} + n_1 \ln \frac{x_{n_1}^2 + R_1 h_0}{x_{n_2}^2 + R_1 h_0} \right] \\ \alpha_{III} = \int_d^{x_{n_2}} d\lambda_{III} = \frac{1}{2} \left[n_1 \ln \frac{x_{n_2}^2 + R_1 h_0}{d^2 + R_1 h_0} - n_2 \ln \frac{(x_{n_2}-d)^2 + iR_1 h_0}{iR_1 h_0} \right] \\ \alpha_{IV} = \int_0^d d\lambda_{IV} = \frac{1}{2} n_1 \ln \frac{d^2 + R_1 h_0}{R_1 h_0} \end{cases} \quad (11)$$

(2) Case 2 ($d < x_{n_1} < l$, $x_{n_2} \leq d$). The accumulated shear strain deviation of the work piece in zone I, II and IV can be calculated by Eq. (12) as follows:

$$\begin{cases} \alpha_I = \int_{x_{n_1}}^l d\lambda_I = \frac{1}{2} \left[n_2 \ln \frac{(l-d)^2 + iR_1 h_0}{(x_{n_1}-d)^2 + iR_1 h_0} - n_1 \ln \frac{l^2 + R_1 h_0}{x_{n_1}^2 + R_1 h_0} \right] \\ \alpha_{II} = \int_d^{x_{n_1}} d\lambda_{II} = \frac{1}{2} \left[n_2 \ln \frac{(x_{n_1}-d)^2 + iR_1 h_0}{iR_1 h_0} + n_1 \ln \frac{x_{n_1}^2 + R_1 h_0}{d^2 + R_1 h_0} \right] \\ \alpha_{IV} = \int_0^d d\lambda_{IV} = \frac{1}{2} n_1 \ln \frac{d^2 + R_1 h_0}{R_1 h_0} \end{cases} \quad (12)$$

(3) Case 3 ($x_{n_1} \geq l$, $x_{n_2} \leq d$). The accumulated shear strain deviation of the work piece in zone II and IV can be calculated by Eq. (13) as follows:

$$\begin{cases} \alpha_{II} = \int_d^l d\lambda_{II} = \frac{1}{2} \left[n_2 \ln \frac{(l-d)^2 + iR_1 h_0}{iR_1 h_0} + n_1 \ln \frac{l^2 + R_1 h_0}{d^2 + R_1 h_0} \right] \\ \alpha_{IV} = \int_0^d d\lambda_{IV} = \frac{1}{2} n_1 \ln \frac{d^2 + R_1 h_0}{R_1 h_0} \end{cases} \quad (13)$$

The total accumulated shear strain deviation in each case is referred as α_T . The curvature caused by the deviation of the upper and lower shear strains of the work piece is expressed as follows:

$$1/r_1 = \alpha_T / l \quad (14)$$

1.3 Plate curvature caused by axial strain

The strain differential of the upper and lower parts of the

rolled piece along x direction can be expressed according to the flow criterion as follows:

$$\begin{cases} d\varepsilon_{x1} = \sigma'_{x1} d\varepsilon_{y1}/\sigma'_{y1} \\ d\varepsilon_{x2} = \sigma'_{x2} d\varepsilon_{y2}/\sigma'_{y2} \end{cases} \quad (15)$$

where ε_{x1} and ε_{x2} are the strain at top and bottom parts of rolled piece along x direction, respectively; σ'_{x1} and σ'_{x2} are the stress bias of the top and bottom parts of rolled piece along the x direction, respectively.

Because $\sigma'_x = \sigma'_{x1} = \sigma'_{x2}$, $\sigma'_y = \sigma'_{y1} = \sigma'_{y2}$, after substituting Eq.(8) into Eq.(15), Eq.(16) and Eq.(17) can be obtained as follows:

$$\begin{cases} d\varepsilon_{x1} = -d\varepsilon_{y1} \\ d\varepsilon_{x2} = -d\varepsilon_{y2} \end{cases} \quad (16)$$

$$\begin{cases} \varepsilon_1 = \int_0^{h_1} \frac{2x}{R_1 h_0 + x^2} dx \\ \varepsilon_2 = \int_0^0 \frac{2(x-d)}{iR_1 h_0 + (x-d)^2} dx \end{cases} \quad (17)$$

with $h_1 = h_0/2 + x^2/2R_1$

$$h_2 = h_0/2 + (x-d)^2/2R_2$$

where ε_1 and ε_2 are the accumulated axial strains along x direction for the top and bottom portions of the plate, respectively. r_2 is the radius of curvature caused by axial strain. Therefore, the curvature caused by the axial strain difference between the upper and lower parts of the work piece is calculated by Eq.(18) as follows:

$$1/r_2 = \frac{10E \int_0^l (\varepsilon_1 - \varepsilon_2) dx}{lh_0} \quad (18)$$

where E is an introduced compensational coefficient to compensate the non-uniform distribution along the thickness. The strain along the thickness is not uniform. The strain difference along the thickness direction of the upper and lower parts can be calculated by Eq.(17). The theoretical modeling of the curvature of snake rolling is carried out on the basis of a large number of simulated practical working conditions, and E is the total compensational coefficient in different situations. It is feasible to predict the curvature within the range as follows: (1) Case 1: $E=(0.0038H^2+0.25d^2-0.048Hd)/(H_{\max}d_{\max})$ when all the four zones exist, and $1.5 \times 10^{-3} \leq E \leq 2.2 \times 10^{-3}$; (2) Case 2: $E=(0.0068H^2+0.37d^2-0.077Hd)/(H_{\max}d_{\max})$ when the three zones exist, and $2.9 \times 10^{-3} \leq E \leq 4.1 \times 10^{-3}$; (3) Case 3: $E=(0.0027H^2+1.4d^2-0.32Hd)/(H_{\max}d_{\max})$ when the two zones exist, and $1.0 \times 10^{-2} \leq E \leq 1.6 \times 10^{-2}$.

1.4 Total plate curvature modeling

r is the total radius of curvature. The total curvature is obtained by combining the curvature caused by shear strain and axial strain, which can be expressed by Eq.(19-21) when the deformation region status belongs Case 1, Case 2, and Case 3, respectively:

$$1/r = \frac{\alpha_I + \alpha_{II} + \alpha_{III} + \alpha_{IV}}{l} + \frac{10E \int_0^l (\varepsilon_1 - \varepsilon_2) dx}{lh_0} \quad (19)$$

$$1/r = \frac{\alpha_I + \alpha_{II} + \alpha_{IV}}{l} + \frac{10E \int_0^l (\varepsilon_1 - \varepsilon_2) dx}{lh_0} \quad (20)$$

$$1/r = \frac{\alpha_{II} + \alpha_{IV}}{l} + \frac{10E \int_0^l (\varepsilon_1 - \varepsilon_2) dx}{lh_0} \quad (21)$$

2 Results and Discussion

The Ansys LS-DYNA is usually used to analyze and simulate the metal forming process and it is suitable to simulate the large plastic deformation process. It can also serve the actual requirement of the metal forming process, and provide guidance for the optimization of the production process, the upgrade of product quality and the improvement of production efficiency, which was verified by many scholars^[27,28]. Therefore, the snake rolling with different radii can be simulated by Ansys software.

The material used in the simulation is 7050 aluminum alloy. The two-dimensional FEM in this research can facilitate the establishment of the model and the simulation of rolling process. The width of the rolled piece is ignored because of the great width/thickness ratio, the elastic deformation of the work rolls is ignored, and the work rolls are defined as rigid body. Plane 162 element is selected in Ansys LS-DYNA. There are many friction models in the Ansys software, and the coulomb friction model is selected.

The process parameters for the simulation and theoretical calculation are shown in Table 1. The curvature index calculated by present model, FEM^[29] and previous experiment^[30] is shown in Fig.3 when the related model is simplified as the asymmetrical rolling. The comparison of the curvature calculated by simulation and theoretical methods is shown in Fig.4. The curvature with different process parameters is obtained by the theoretical model established in this research. The calculat-

Table 1 Process parameters of simulation model and theoretical calculation

Type	Parameter	Value
Work roll	Top work roll radius/mm	500~521
	Bottom work roll radius/mm	525
	Roll offset/mm	12~24
	Angular velocity/rad·s ⁻¹	2.476
	Elastic modulus/GPa	206
Rolled plate	Poisson ratio	0.25
	Plate width/mm	3000
	Plate length/mm	2000
	Initial thickness/mm	220~300
	Rolling reduction/mm	30~50
	Yield stress/MPa	77
	Tangent modulus/MPa	12.8
	Elastic modulus/GPa	34
	Poisson ratio	0.33
	Roll speed/m·s ⁻¹	1.3
Others	Dynamic friction coefficient	0.35
	Static friction coefficient	0.40

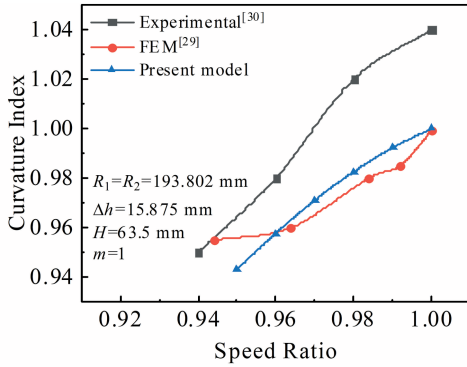


Fig.3 Comparison of curvature index obtained by different methods

ed results are shown in Fig.5~8.

The curvature index in Fig. 3 is referred as $K = (r-h_0/2)/(r+h_0/2)$. The roll radius ratio is a factor to greatly affect the position of the neutral points and the length of the cross shear zone. The main reason for the plate bending is the existence and length of the cross shear zone. So the curvature index can verify the precision of present model indirectly. The present model can be simplified to synchronous rolling when $R_1=R_2$, and the curvature index is 1 in the ideal state. Δh is total rolling reduction. The results calculated by the present model are in very good agreement with those obtained by FEM and experiment. The curvature affecting law and its calculation during the snake rolling with different roll radii need further analysis and verification.

The curvatures calculated by the numerical and theoretical methods are shown in Fig.4. The maximum relative errors are 10.71% and 3.17% in Fig.4a and 4b, respectively; the minimum relative errors are 1.01% and 0.34% in Fig.4a and 4b, respectively. The relative error of the established model is less than 11% compared with the simulation results. Therefore, the accuracy of the theoretical model is acceptable.

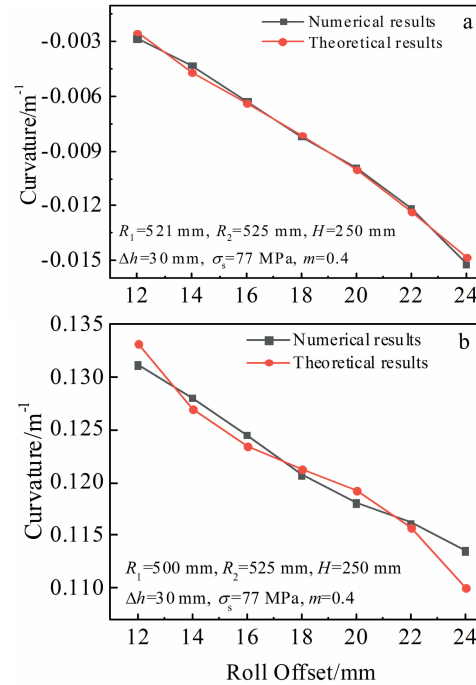


Fig.4 Comparison of numerical and theoretical curvatures with different top work roll radii: (a) $R_1=521$ mm and (b) $R_1=500$ mm

It can be seen from Fig.4 that the two curves calculated by the numerical and theoretical methods are relatively close when $R_1=521$ mm. The two curves calculated by numerical and theoretical methods have a very small distance when the top work roll radius is 500 mm. However, the plate is close to a straight state and the curvature radius is large due to the roll radius ratio is relatively small. Therefore, although the two curves are close, the maximum relative error is 10.71%.

Fig.5a is the curvature determined by the theoretical model when $R_1=521$ mm. The deformation region consists of zone I,

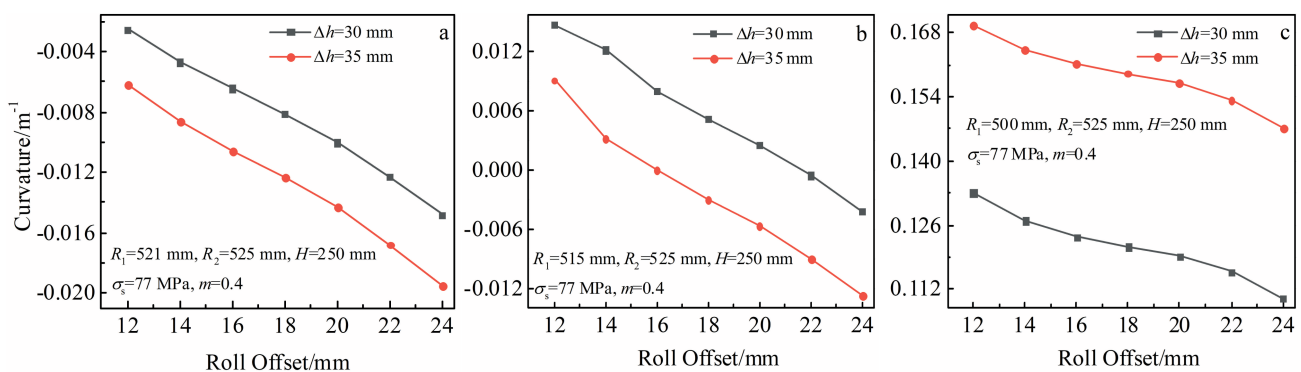


Fig.5 Relationship between curvature and roll offset with different top work roll radii: (a) $R_1=521$ mm, (b) $R_1=515$ mm, and (c) $R_1=500$ mm

II, III and IV according to the calculated x_{n_1} and x_{n_2} . The curvature is less than zero in Case 1, which indicates that the rolled work piece tends to be bent downward. The absolute value of the curvature increases as the roll offset increases, and the downward bending trend appears.

The curvature caused by the shear strain makes the work piece bent upward when the roll radius ratio is small, and the value is greater than zero. The curvature caused by the axial strain makes the work piece bent downward, and the value is less than zero. But the curvature caused by the axial strain is larger than that caused by the shear strain in this situation. Therefore, the total curvature is less than zero, and the plate downward trend is more obvious as the roll offset augments. It can also be known from Fig.5 that the absolute value of curvature increases as the rolling reduction increases. So the rolling reduction is an important factor to adjust the curvature after the snake rolling.

Fig.5b shows the curvature affecting law with the effect of the roll offset under different rolling reduction when R_1 is 515 mm. The work piece tends to be bent upward when the roll offset is small, and then it tends to be bent downward with the augment of roll offset. The essence from the theoretical model is that the deformation region consists of zone I, II and IV at this time, and the three integration intervals are $(0, d)$, (d, x_{n_1}) and (x_{n_1}, l) . The x_{n_1} does not change drastically as the roll offset augments, and the curvature caused by the shear strain does not change too much. But the curvature caused by the axial strain increases with the increase of roll offset. The curvature caused by the axial strain makes the work piece bent downward. Therefore, the rolled plate bends downward.

Fig.5c shows the curvature affecting law with the effect of the roll offset under different rolling reductions when R_1 is 500 mm. The curvature is greater than zero, and it can be known that the work piece tends to be bent upward. The curvature reduces with the increase of roll offset. The work piece tends to be bent upward. However, the bending extent reduces with the increase of roll offset. The essence from the theoretical model is that the deformation region consists of zone II and IV in this situation, and the two integration intervals are $(0, d)$ and (d, l) . The curvature caused by the shear strain does not alter drastically as the roll offset augments. The curvature caused by the axial strain augments as the roll offset augments. The curvature caused by axial strain makes the work piece bent downward, which counteracts the upward bending trend of the work piece.

Fig. 6 shows the curvature determined by the theoretical model with different roll radius ratios. As shown in Fig.6, the curvature changes from negative to positive as the roll radius ratio augments with fixed roll offset. The curvature is progressively bent upward from downward. The essence from the theoretical model is that the roll radius ratio produces an effect on the position of x_{n_1} and x_{n_2} , thereby affecting the curvature caused by the shear strain. The curvature caused by the shear strain augments progressively with the increase of roll radius ratio, and the value is positive. The axial strain makes the

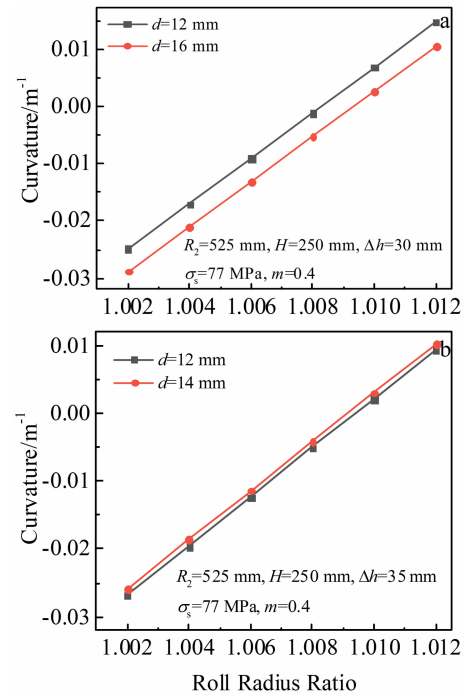


Fig.6 Relationship between curvature and roll radius ratio with different Δh : (a) $\Delta h=30$ mm and (b) $\Delta h=35$ mm

work piece bent downward and the value is negative with a fixed roll offset. So the total curvature changes from negative to positive.

Fig. 7 shows the curvature affecting law with the effect of

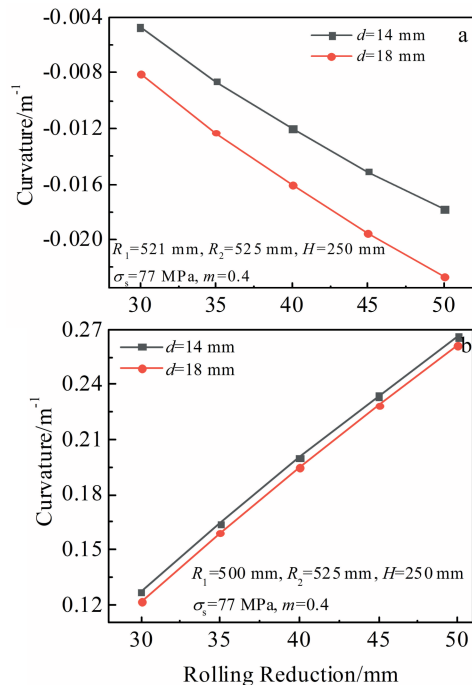


Fig.7 Relationship between curvature and rolling reduction with different top work roll radii: (a) $R_1=521$ mm and (b) $R_1=500$ mm

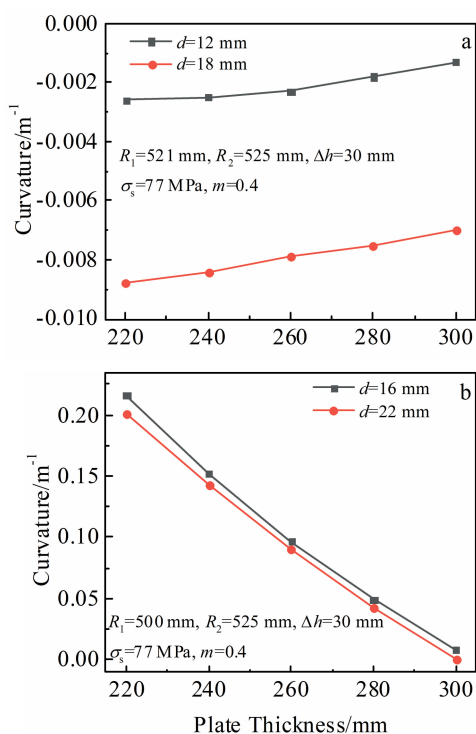


Fig.8 Relationship between curvature and initial work piece thickness with different top work roll radii: (a) $R_1=521$ mm and (b) $R_1=500$ mm

the rolling reduction. The absolute value of work piece curvature increases as the rolling reduction augments, regardless of the roll radius ratio. The work piece tends to be bent downward when R_1 is 521 mm, and it tends to be bent upward when R_1 is 500 mm. The work piece is bent more as the rolling reduction augments.

Fig.8 shows the curvature affecting law with the effect of the initial work piece thickness. The absolute value of work piece curvature reduces with the increase of initial work piece thickness. The value is close to zero, indicating that the work piece is straight. The work piece tends to be bent downwards when R_1 is 521 mm, and it tends to be bent upwards when R_1 is 500 mm. The work piece is less likely to bend as the initial work piece thickness augments.

3 Conclusions

1) The roll radius ratio has a great influence on the position of neutral points, and then the length of the cross shear zone is affected. The main reason of the bending of work piece is the existence and the length of the cross shear zone. There are three situations for calculating the curvature as a result of the shear strain.

2) The theoretical model of the curvature for the snake rolling with different roll radii is established by the slab method on the basis of different components of the deformation region. The calculated results are in very good agreement with

the results from finite element method (FEM) and experiment. Comparison of the results calculated by the theoretical model and the FEM shows that the theoretical model accurately predicts the curvature during the snake rolling process.

3) The curvature as a result of the shear strain causes the work piece bent upward. The curvature as a result of the axial strain makes the work piece bent downward. The curvature changes from negative to positive as the roll radius ratio augments. The work piece tends to be bent upward from downward as the roll radius ratio augments.

4) The process parameters in the snake rolling produce a certain effect on the curvature after snake rolling. The obtained affecting law provides an important theoretical basis for the plate snake rolling production with good shape.

References

- 1 Yuan X K, Cui L. *Rare Metal Materials and Engineering*[J], 2019, 48(9): 2768
- 2 Ren J P, Song R G. *Rare Metal Materials and Engineering*[J], 2020, 49(4): 1159
- 3 Liu L L, Pan Q L, Wang X D et al. *Journal of Alloys and Compounds*[J], 2018, 735: 261
- 4 Jin H, Lloyd D J. *Materials Science and Engineering A*[J], 2007, 465(1): 267
- 5 Zuo Y B, Fu X, Cui J Z et al. *Transactions of Nonferrous Metals Society of China*[J], 2014, 24(7): 2220
- 6 Kim W J, Yoo S J, Lee J B. *Scripta Materialia*[J], 2009, 62(7): 451
- 7 Ko Y G, Suharto J, Lee J S et al. *Metals and Materials International*[J], 2013, 19(3): 603
- 8 Cui Q, Ohori K. *Materials Science and Technology*[J], 2000, 16(10): 1095
- 9 Wronski M, Wierzbanski K, Bacroix B et al. *Materials Science and Engineering*[J], 2015, 82(1): 1
- 10 Jin H, Lloyd D J. *Scripta Materialia*[J], 2004, 50(10): 1319
- 11 Angella G, Dellasega D, Farè S et al. *Metallurgical Science and Technology*[J], 2010, 28(1): 22
- 12 Anders D, Münker T, Artel J et al. *Journal of Materials Processing Technology*[J], 2012, 212(6): 1387
- 13 Gong W, Pang Y H, Liu C R et al. *Journal of Iron and Steel Research International*[J], 2010, 17(1): 22
- 14 Hao L, Di H S, Gong D Y. *Journal of Iron and Steel Research International*[J], 2013, 20(5): 34
- 15 Farhatnia F, Salimi M, Movahhedy M R. *Journal of Materials Processing Technology*[J], 2006, 177(1-3): 525
- 16 Kadkhodaei M, Salimi M, Poursina M. *International Journal of Mechanical Sciences*[J], 2006, 49(5): 622
- 17 Qwamizadeh M, Kadkhodaei M, Salimi M. *International Journal of Advanced Manufacturing*[J], 2012, 61(1-4): 227
- 18 Qwamizadeh M, Kadkhodaei M, Salimi M. *International Journal of Advanced Manufacturing Technology*[J], 2014, 73(1-4): 521
- 19 Salimi M, Qwamizadeh M. *Journal of Materials Processing Technology*[J], 2004, 150(3): 215
- 20 Salimi M, Sassani F. *International Journal of Mechanical Sciences*[J], 2002, 44(9): 1999
- 21 Afrouz F, Parvizi A. *Journal of Manufacturing Process*[J], 2015, 20: 162
- 22 Ling L Y, Tang J G, Liu W H et al. *Journal of Central South University*[J], 2017, 48(9): 2279 (in Chinese)

- 23 Zhang T, Wu Y X, Gong H et al. *Transactions of Nonferrous Metals Society of China*[J], 2014, 27(7): 2150
- 24 Jiang L Y, Zhao C J, Yuan G et al. *Metallurgical Research and Technology*[J], 2016, 113(3): 309
- 25 Yang J X, Li S Y, Liu J et al. *Journal of Materials Processing Technology*[J], 2017, 240: 274
- 26 Jiang L Y, Zhen T, Yuan G et al. *Metallurgical Research and Technology*[J], 2020, 117(3): 301
- 27 Jiang L Y, Meng Q C, Zhao C J et al. *Mathematical Problems in Engineering*[J], 2018: 7 807 580
- 28 Pattarawadee P, Wasawat N, Nirut N. *Materials Research Express*[J], 2020, 7(5): 56 518
- 29 Shivpuri R, Chou P C, Lau C W. *International Journal of Mechanical Sciences*[J], 1988, 30(9): 625
- 30 Buxton S A E, Browning S C. *Journal of Mechanical Engineering Science*[J], 1972, 14(4): 245

不同变形区组成下铝合金厚板蛇形轧制板曲率建模分析

江连运¹, 黄金博¹, 甄涛¹, 乐启焯², 马立峰¹

(1. 太原科技大学 机械工程学院, 山西 太原 030024)

(2. 东北大学 材料电磁过程研究教育部重点实验室, 辽宁 沈阳 110819)

摘要: 蛇形轧制作为一种新型的轧制工艺为高性能厚铝板生产提供了一种新方法, 但是传统的异步轧制弯曲曲率模型不能用于蛇形轧制, 蛇形轧制缺少精准的轧后曲率计算模型。根据变形区的特征及中性点的位置, 确定了变形区组成及其存在边界条件; 塑性变形区最多可分成4个区, 对不同组成情况的变形区进行了分析, 建立了各种情况下单位压力和上、下部分累积剪应变偏差模型, 在此基础上建立了剪切应变引起的弯曲曲率模型, 根据流动准则建立了轴向应变引起的弯曲曲率模型, 最终建立了不同辊径比下的蛇形轧制的弯曲曲率模型。考虑到厚度方向变形的不均匀性, 在建模过程中引入均匀系数 E , 使模型更加精确。采用Ansys模拟和实验数据进行了模型精度的间接验证。结果表明, 与模拟和间接实验结果相比, 最大和最小相对误差分别为10.71%和0.34%, 证实了模型精度, 可应用于弯曲曲率预测及控制; 同时研究了不同工艺参数(偏移量、辊径比、压下量、工件初始厚度等)对弯曲曲率的影响规律。研究结果为厚规格铝板蛇形轧制生产提供重要理论和技术支持。

关键词: 蛇形轧制; 曲率; 中性点; 剪切应变; 轴向应变

作者简介: 江连运, 男, 1985年生, 博士, 副教授, 太原科技大学机械工程学院, 山西 太原 030024, 电话: 0351-2776763, E-mail: jiangly@tyust.edu.cn